Journal of Alloys and Compounds 525 (2012) 14–21

Contents lists available at SciVerse ScienceDirect

Journal of Alloys and Compounds

journal homepage: www.elsevier.com/locate/jallcom

$La_{0.90}Dy_{0.05}Nb_2O_7$ nanosheet phosphor and its multilayer films with enhanced host excitation-mediated photoluminescence

Li-Mei Fu, Bi-Zhou Lin*, Yi-Lin Chan, Ou Zhang, Bin Li, Hu Qu

Key Laboratory for Functional Materials of Fujian Higher Education, College of Materials Science and Engineering, Huaqiao University, Xiamen 361021, China

ARTICLE INFO

Article history:
Received 16 January 2012
Received in revised form 30 January 2012
Accepted 30 January 2012
Available online xxx

Keywords:
Dy^{3+}
Perovskite
Ln-photoactivated phosphors
Layer-by-layer assembly technology
Nanosheets
Multilayer films
Photoluminescence

ABSTRACT

$La_{0.90}Dy_{0.05}Nb_2O_7$ nanosheets were achieved by exfoliating a layered compound $HLa_{0.90}Dy_{0.05}Nb_2O_7$. Multilayer films composed of the exfoliated nanosheets were prepared by a layer-by-layer deposition technology, which were subsequently heat-treated at 450 °C and exposed under ultraviolet light to obtain the polymer-free nanosheet films, respectively. The resulting $La_{0.90}Dy_{0.05}Nb_2O_7$ nanosheet suspension and its films exhibit intense emission by the host excitation and negligibly low emission by the direct Dy^{3+} excitation, whereas the photoluminescence emissions of the bulk precursors are largely dominated by the direct Dy^{3+} excitation rather than the host excitation. The comparison between the excitation spectra and the bandgap absorption spectra indicates that the enhanced host excitation-mediated photoluminescence of $La_{0.90}Dy_{0.05}Nb_2O_7$ nanosheet results from the efficient energy transfer from the O–Dy charge-transfer transition to Dy^{3+} within the nanosheet, and that the intensive emission of the multilayer films is attributed to the energy transfer from both of the O–Dy charge-transfer transition and the O–Nb network to Dy^{3+}. Dy^{3+} in the $La_{0.90}Dy_{0.05}Nb_2O_7$ nanosheet and the nanosheet-based films gives two emission peaks at around 480 and 576 nm and the blue emission is prominent in the film form.

1. Introduction

In the past decades, two-dimensional nanosheets, prepared by delaminating layered oxides in a soft-chemical route, have been extensively explored [1–9]. An intriguing aspect of the exfoliated oxide nanosheets is their high crystallinity inherited from layered precursors, and an individual nanosheet can be considered as a two-dimensional single crystal with a thickness of subnano- to nanometer range and a lateral size of micrometers range. These oxide nanosheets were found to exhibit distinctive structure diversity, interesting photophysical and photochemical properties. Several studies demonstrated that the photoluminescence (PL) emissions from Ln (rare earth)-photoactivated oxide nanosheets in fluid suspensions are dominated by nanosheet host excitation rather than direct Ln photoactivator excitation, whereas the emissions from all their bulk precursors are dominated by direct Ln excitation [5,10–15]. For an Ln-containing phosphor with well-predictable mission wavelengths from the intra-4f transitions, its direct Ln excitation wavelength is often nontunable (corresponding to the characteristic f–f transitions of the Ln photoactivator), but its host excitation wavelengths can be tuned on the bias of the host absorption properties. Ozawa et al. reported the PL emissions of Eu^{3+}- and Sm^{3+}-doped $LaNb_2O_7$ nanosheets in fluid suspensions are predominated by the energy transfer from the oxide nanosheet hosts to the Ln photoactivators [12,13]. $LaNb_2O_7$ perovskite nanosheet can be considered as an ideal candidate host nanosheet for Ln-photoactivated phosphors. The absorption onset wavelengths of the Eu^{3+}- and Sm^{3+}-doped $LaNb_2O_7$ nanosheets and the Eu^{3+}-doped $KLaNb_2O_7$ bulk sample are around 370 nm [12,13,16], whereas the GaN-based solid state lighting requires phosphors that can be effectively excited in the 250–400 nm range [17]. Therefore, it is worthwhile to investigate the PL properties of Ln-doped $LaNb_2O_7$ nanosheets, shedding light on the new generation solid state lighting based on GaN.

Due to their negative charged nature, the exfoliated oxide nanosheets can be flocculated with positively changed species by the electrostatic self-assembly deposition (ESD) to form nanocomposites [1]. In particular, it is attractive to use them to fabricate multilayer composite films on a glass substrate through the layer-by-layer (LBL) assembly technology, based on the alternate adsorption with suitable polymeric cations [18–24]. After followed by ultraviolet light exposure or heat treatment, the organic cations will be decomposed completely, which leads to the formation of transparent polymer-free nanosheet multilayer films deposited on the substrate [22–24]. To the best of our knowledge, only the red Eu^{3+} and Sm^{3+} emissions of doped $LaNb_2O_7$ nanosheets in fluid suspensions have been reported [12,13], the assembly films of Ln-doped $LaNb_2O_7$ nanosheets have been unexplored so far. It is very

* Corresponding author. Fax: +86 592 6162221.
E-mail addresses: bzlin@hqu.edu.cn, beerlin@hqu.edu.cn (B.-Z. Lin).

0925-8388/$ – see front matter © 2012 Elsevier B.V. All rights reserved.
doi:10.1016/j.jallcom.2012.01.159

interesting to evaluate the PL emissions of nanosheets in such solid state form for solid state lighting.

Among the Ln photoactivators, Dy^{3+} is particularly interesting due to its visible luminescence in the blue (470–500 nm, $^4F_{9/2} \rightarrow {}^6H_{15/2}$) and yellow (570–600 nm, $^4F_{9/2} \rightarrow {}^6H_{13/2}$) wavelength regions. The latter one belongs to the hypersensitive transition, which is strongly influenced by the environment [25–27]. In the present paper, we report the preparation and PL properties of Dy^{3+}-photoactivated $La_{0.90}Dy_{0.05}Nb_2O_7$ perovskite nanosheet and its multilayer films. Their characterization results are compared with those of the bulk precursors $KLa_{0.90}Dy_{0.05}Nb_2O_7$ and $HLa_{0.90}Dy_{0.05}Nb_2O_7$.

2. Experimental

2.1. Reagents and materials

All reagents were of analytical grade and used without further purification. Milli-Q ultrapure water with a resistivity of 18.2 MΩ cm was used throughout the experiments. The host layered compound Dy^{3+}-doped $KLaNb_2O_7$, $KLa_{0.90}Dy_{0.05}Nb_2O_7$, was prepared by a conventional solid-state reaction of a mixture of K_2CO_3:La_2O_3:Nb_2O_5:Dy_2O_3 in the molar ratio of 1.15:0.90:2.00:0.05 at 1150 °C for 24 h in a corundum crucible, similar to the procedures of $KLa_{0.90}Eu_{0.05}Nb_2O_7$ and $KLa_{0.90}Sm_{0.05}Nb_2O_7$ analogs [12,13]. The 15% excess of K_2CO_3 was used in order to compensate for its loss by evaporation during the heating reaction. It was found that the single-phase stoichiometric bulk precursor $KLaNb_2O_7$/Dy^{3+} could not be synthesized. As reported in Refs. [12,28], the starting component amount Ln_2O_3 (Ln = La or Dy) had to be reduced from the stoichiometric one for $KLnNb_2O_7$ in order to avoid the coproduction of impurity phases like $LnNbO_4$. In case of 5% Dy^{3+} doping, 5% reduction of Ln was necessary to obtain the single-phase precursor $KLa_{0.90}Dy_{0.05}Nb_2O_7$.

The bulk layered compound was converted into its acid phase (designated as $HLa_{0.90}Dy_{0.05}Nb_2O_7$) by stirring vigorously a $KLa_{0.90}Dy_{0.05}Nb_2O_7$ suspension in 3 M HNO_3 solution at RT for 6 days. During the proton exchange reaction, the acid solution was replaced with a fresh one every 2 days. The resultant solid product was centrifuged, washed with deionized water and air-dried at room temperature for 24 h. The protonated powder was exfoliated into lanthanoniobate nanosheets in a tetrabutylammonium hydroxide (TBAOH) solution with a butylamine/H^+-niobate molar ratio of 2:1. In a typical reaction, 0.5 g $HLa_{0.90}Dy_{0.05}Nb_2O_7$ was added to 250 mL 15% TBAOH aqueous solution and ultrasonicated at RT for 2 h. Subsequent centrifugation at 4500 rpm for 30 min yielded an opalescent colloidal suspension of $La_{0.90}Dy_{0.05}Nb_2O_7$ nanosheet with a concentration of about 10^{-3} M. Then the pH value of colloidal suspension was adjusted to 9.0 by 0.5 M HNO_3 carefully.

2.2. Preparation of flocculation and film

The flocculated nanohybrid PEI/$La_{0.90}Dy_{0.05}Nb_2O_7$ was performed by adding 20 mL polyethylenimine (PEI) solution (2.5 g L^{-1}, pH 9.0) into 200 mL as-prepared $La_{0.90}Dy_{0.05}Nb_2O_7$ nanosheet suspension under vigorous stirring. Driven by electrostatic interaction between the negatively charged nanosheets and positively charged PEI, the mixing immediately resulted in a flocculated sludge. The sludge was separated by centrifugation at 3500 rpm, washed several times with ethanol–water mixed solvent (1:1 in volume) to remove excess PEI and other soluble products. The resulting product was dried under vacuum at 80 °C for 12 h. For comparison, a flocculated sample without PEI loading was prepared by acidizing the suspension and designated as e-$HLa_{0.90}Dy_{0.05}Nb_2O_7$.

Deposition of $La_{0.90}Dy_{0.05}Nb_2O_7$ nanosheets and PEI on Quartz glass was achieved by alternately exposing the substrate in the positively charged PEI and the negative nanosheets colloid through a LBL technique. Quartz glass substrates were cleaned by ultrosonication in acetone, followed by treatment in a bath of methanol/HCl (1:1 in volume) and then concentrated H_2SO_4 for 30 min each. The surface-cleaned substrate was first immersed in a PEI solution (25 g L^{-1}, pH 9.0) for 20 min. After being washed thoroughly with pure water and drying under a N_2 stream, the PEI-coated substrate was dipped into the nanosheet colloidal suspension (2×10^{-5} M, pH 9.0) for 20 min, followed by washing with copious water and drying under a N_2 stream. The above procedure was repeated n times to obtain a multilayer film of $(PEI/La_{0.90}Dy_{0.05}Nb_2O_7)_n$.

To obtain polymer-free phosphors, the as-prepared multilayer films were heated in air at 450 °C for 2 h with an increment of 2 °C min^{-1} and exposed under a 300 W low-pressure Hg lamp (λ_{max} = 254 nm) irradiation for 12 h, respectively. The resulting polymer-free phosphors were allowed to evaluate their PL properties.

2.3. Sample characterization

Powder X-ray diffraction (XRD) patterns were recorded at RT on a Bruker D8 Advance diffractometer using Ni-filtered Cu Kα radiation (λ = 1.5406 Å) under the accelerating voltage of 36 kV at a scanning rate of 4° at 2θ min^{-1} from 2° to 50°. Elemental compositions of the as-prepared bulk compound were analyzed with a Leeman Prodigy ICP-OES analyzer. The surface topography of the films was examined using a Veeco Nanoscope 3D atomic force microscope (AFM) in the tapping mode with a silicon-tip cantilever (15 N m^{-1}). Simultaneous TG–DTA measurements were performed from RT to 900 °C at a rate of 10 °C min^{-1} on a Shimadzu DTG-60H thermalanalyzer in N_2 flow. UV–vis absorption spectra of the diluted nanosheet suspensions were measured on a Shimadzu UV-2450 spectrometer. Diffuse reflectance spectra were recorded on a Shimadzu UV-2550 spectrometer equipped with an integrating sphere 60 mm in diameter using $BaSO_4$ as a reference, and the reflectance spectra were converted to the absorption spectra by the Kubelka–Munk method. Both photoluminescence excitation and emission spectra were obtained on an Edinburgh FLS920 fluorescence spectrometer at RT. The excitation source is a 450 W Xenon lamp and the spectral resolution of the spectrofluorometer was 0.05 nm.

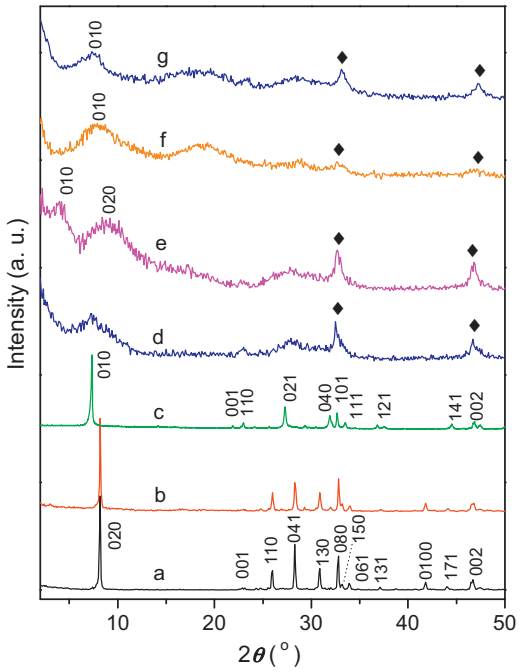

Fig. 1. Power XRD patterns of layered compounds $KLaNb_2O_7$ (a) and $KLa_{0.90}Dy_{0.05}Nb_2O_7$ (b), protonated $HLa_{0.90}Dy_{0.05}Nb_2O_7 \cdot nH_2O$ (c), restacked e-$HLa_{0.90}Dy_{0.05}Nb_2O_7$ (d), as-prepared PEI/$La_{0.90}Dy_{0.05}Nb_2O_7$ flocculation before (e), and after heat-treated at 450 °C (f) and after UV light exposure (g). Closed squares represent the in-sheet characteristic peaks of $La_{0.90}Dy_{0.05}Nb_2O_7$ sheets.

3. Results and discussion

3.1. Characterization of flocculation

Comparison of the XRD profiles between the layered lanthanoniobate $KLaNb_2O_7$ and its Dy^{3+}-doped phase $KLa_{0.90}Dy_{0.05}Nb_2O_7$ is documented in Fig. 1a and b. Their patterns are very similar and can be indexed to the orthorhombic cell with C222 space group and a = 3.9060, b = 21.6031, c = 3.8879 Å [28], which reflects that their structures consist of stacked single perovskite-type layers interspersed with K^+. The strong and sharp (0 2 0) diffraction of $KLa_{0.90}Dy_{0.05}Nb_2O_7$ at 8.16° with d-spacing of 1.08 nm indicates that the well-ordered layered structure was formed. The protonated bulk compound exhibits an intense reflection at around 7.28° (Fig. 1c). The corresponding d-spacing of 1.21 nm is close to the lattice parameter along the intersheet direction of the hydrated analogous protonated phase $HLaNb_2O_7 \cdot nH_2O$ [29]. In the undoped analogous phase $KLaNb_2O_7$, stacking of each sheet is shifted by 1/2 unit cell (perovskite unit) toward one of the intralayer directions, whereas no such shift of stacking layers was observed and the apical oxygen ions of the adjacent sheets are eclipsed in the case of its protonated form [28]. The unit cell of the as-prepared bulk compound contains two perovskite-type sheets along the intersheet direction (the b axis), whereas that of the protonated compound

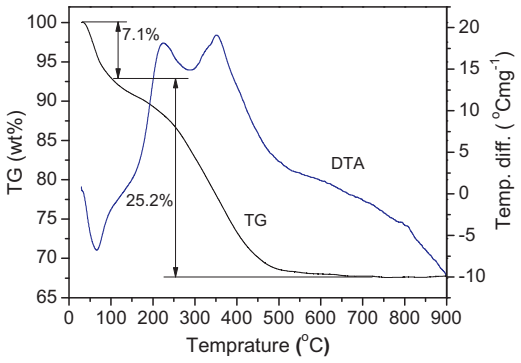

Fig. 2. Simultaneous TG–DTA curves of PEI/$La_{0.90}Dy_{0.05}Nb_2O_7$ nanocomposite.

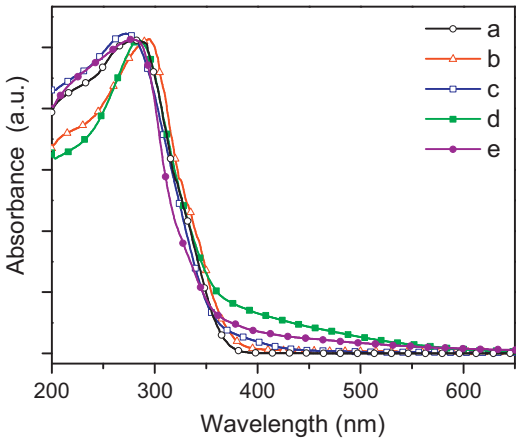

Fig. 3. Diffuse reflection spectra of $KLa_{0.90}Dy_{0.05}Nb_2O_7$ (a), protonated $HLa_{0.90}Dy_{0.05}Nb_2O_7$ (b), PEI/$La_{0.90}Dy_{0.05}Nb_2O_7$ flocculation before (c), and after heat-treated at 450 °C (d) and after UV light exposure (e).

contains only one perovskite-type sheet [29]. It is rational to expect that the slightly Dy^{3+}-doped phase $KLa_{0.90}Dy_{0.05}Nb_2O_7$ and its protonated phase crystallize similarly to their undoped analogs. After the exfoliated $La_{0.90}Dy_{0.05}Nb_2O_7$ nanosheets were restacked by acidizing the suspension at low pH < 3, the main reflections of e-$HLa_{0.90}Dy_{0.05}Nb_2O_7$ were observed to be located at similar positions to those of $HLa_{0.90}Dy_{0.05}Nb_2O_7$ (Fig. 1d). Considering the smaller radius of H^+ with respect to that of K^+, the larger intersheet distances in the protonated phases than in $KLa_{0.90}Dy_{0.05}Nb_2O_7$ can be reckoned as a result of a monolayer arrangement of the intercalated water molecules along with the protons between the sheets, similar to those previously found in other restacked oxide sheets [9,29–31]. The observation implies that $HLa_{0.90}Dy_{0.05}Nb_2O_7$ was almost completely exfoliated into single nanosheets after reaction with TBAOH.

Upon adding PEI solution, the exfoliated sheets were restacked, leading to the formation of PEI/$La_{0.90}Dy_{0.05}Nb_2O_7$. As shown in Fig. 1e, the reflections at 3.97° and 8.34°, indexed as (0 0 1) and (0 0 2) reflections respectively, were observed. The intersheet spacing was determined to be 2.22 nm. The distance between the apical oxygen atoms within a $LaNb_2O_7$ sheet is 0.790 nm from the crystallographic data of $KLaNb_2O_7$ [28]. Taking the van der Waals radius of O atom (0.140 nm), the thickness of the lanthanoniobate sheet can be evaluated as 1.07 nm. Deducting from this thickness, the intersheet expansion of PEI/$La_{0.90}Dy_{0.05}Nb_2O_7$ was determined to be 1.15 nm, which evidently demonstrates that PEI is intercalated into the intersheet region between the sheets. After heat treatment at 450 °C for 2 h, the (0 1 0) reflection of PEI/$La_{0.90}Dy_{0.05}Nb_2O_7$ was shifted to a higher angle 7.89°, corresponding to *d*-spacing of 1.12 nm (Fig. 1f). On the other hand, after UV light exposure, the (0 1 0) angle and its corresponding *d*-spacing were observed to be 7.42° and 1.19 nm, respectively (Fig. 1g). During the heat and UV light treatment, the intercalated organic components between the sheets were decomposed, the residue was curtained as NH_4^+ and/or oxonium ions, along with water molecules [3,21,32]. The nearly completed evaporation of water molecules gave rise to the slightly smaller *d*-spacing in the heat-treated sample than that in the UV treated sample.

Fig. 2 shows the TG–DTA results of the as-prepared PEI/$La_{0.90}Dy_{0.05}Nb_2O_7$ nanocomposite flocculation. Its weight loss was found to be extended over a wide temperature range due to the combination of several factors such as dehydration and decomposition. The first step below 110 °C with a weight loss of 7.1% and an endotherm at 66 °C can be attributed contributed to the dehydration of the adsorbed H_2O on the surface and within the material. The second step between 110 and 700 °C with a loss of 25.2% is due to the carbonized decomposition of organic components. The exothermic peak at 225 °C can be mostly attributed to the decomposition of the residual TBA^+, while the peak at 353 °C might be raised from the pyrolysis of the interlayered PEI molecules. The results are consistent with the XRD results of PEI/$La_{0.90}Dy_{0.05}Nb_2O_7$ heated at 450 °C. There seemed to be no distinct weight loss beyond 500 °C, but there might have been the slow transformation of the lanthanoniobate sheets into $Ln_{1/3-\delta}NbO_3$ and $LnNbO_4$ at around 800 °C with a small exotherm, similar to that previously reported [12,13]. This fact suggests that the heat-treated temperature of PEI/$La_{0.90}Dy_{0.05}Nb_2O_7$ nanocomposite powders or films must be between 353 and 500 °C to obtain polymer-free phosphors and to avoid destroying the layered structure of $La_{0.90}Dy_{0.05}Nb_2O_7$ nanosheet. Therefore, 450 °C was employed as the heat-treated temperature in the present study.

Diffuse reflection spectra of $KLa_{0.90}Dy_{0.05}Nb_2O_7$, $HLa_{0.90}Dy_{0.05}Nb_2O_7$, PEI/$La_{0.90}Dy_{0.05}Nb_2O_7$ and its heat-treated and UV-exposed products are shown in Fig. 3. The absorption edge of PEI/$La_{0.90}Dy_{0.05}Nb_2O_7$ nanocomposite was observed at 425 nm, which is red-shifted with respect to those of the bulk precursors $KLa_{0.90}Dy_{0.05}Nb_2O_7$ and $HLa_{0.90}Dy_{0.05}Nb_2O_7$, whose absorption edges are 381 and 398 nm, respectively. The red shift of PEI/$La_{0.90}Dy_{0.05}Nb_2O_7$ was probably attributed to the charge-transfer (CT) transition of O → Dy, similar to that of the $La_{0.90}Dy_{0.05}Nb_2O_7$ nanosheet suspension (discussed below). After heat treatment and UV-exposure, the absorption peak at about 280 nm remained almost unchanged while the absorption edge was further red-shifted. The lattice strain from the doped Dy^{3+} is prominent in such treated samples, and the dopant effect may result in this red shift.

3.2. Characterization of nanosheet

It was found that the $La_{0.90}Dy_{0.05}Nb_2O_7$ nanosheet colloidal suspension is stable at the pH range of 4–10. A typical AFM image of $La_{0.90}Dy_{0.05}Nb_2O_7$ nanosheets adsorbed on a PEI-coated quartz glass demonstrates that the unilamellar nanosheets have an average thickness of ~1.13 nm with several hundred nanometers in lateral size (Fig. 4). This value is closed to the estimated value (1.07 nm) from the crystallographic data [28]. The slightly larger value might come from the adsorption of oxonium and TBA^+ ions, which is similar to other oxide nanosheets [13,31]. These nanosheets are irregular in shape, suggesting breakage or fracture of the sheets during delamination process.

The UV–vis absorption spectrum of the nanosheet colloidal suspension is shown in Fig. 5, showing two peaks at 230 and 320 nm. In the nanosheets, the conduction band is composed of the 3d orbits in Nb^{5+} and the 4d and 4f orbits in Ln^{3+}, and the valence band consists of the 2p orbits in O^{2-}. The conduction band of

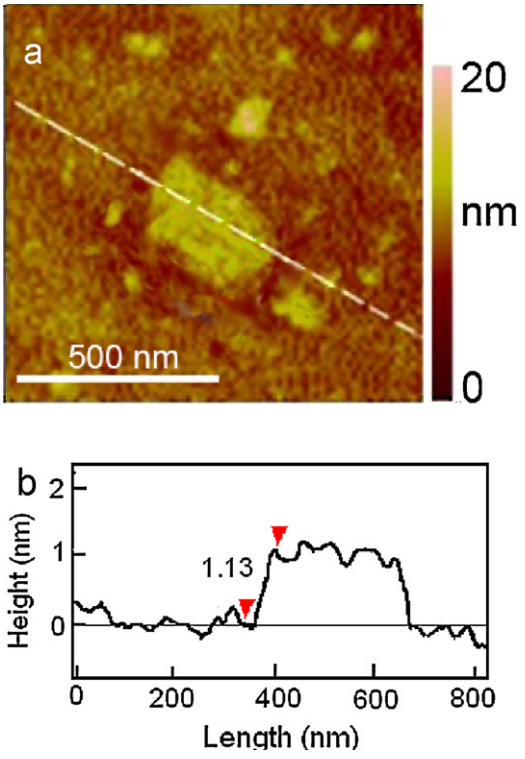

Fig. 4. Tapping-mode AFM images of $La_{0.90}Dy_{0.05}Nb_2O_7$ nanosheet film (a) and its cross-sectional profile (b).

the Nb–O system position in a higher position than that of Ln–O system [5,33]. The absorption centered at 230 and 320 nm can thus be ascribed to the photogenerated electrons excited from the valence band to the conduction band components contributed by Nb^{5+} and Ln^{3+}, respectively. The absorbance of the exfoliated nanosheet suspension was found to exhibit a Lambert–Beer's relationship (the top insert of Fig. 5). The molar extinction coefficients were determined as $2.11 \times 10^4\ mol^{-1}\ dm^3\ cm^{-1}$ at 230 nm and $2.09 \times 10^3\ mol^{-1}\ dm^3\ cm^{-1}$ at 320 nm, respectively. The bottom insert of Fig. 5 displays a typical photograph of the translucent opalescent colloidal suspension. Clear Tyndall light scattering was reflected from its colloidal nature.

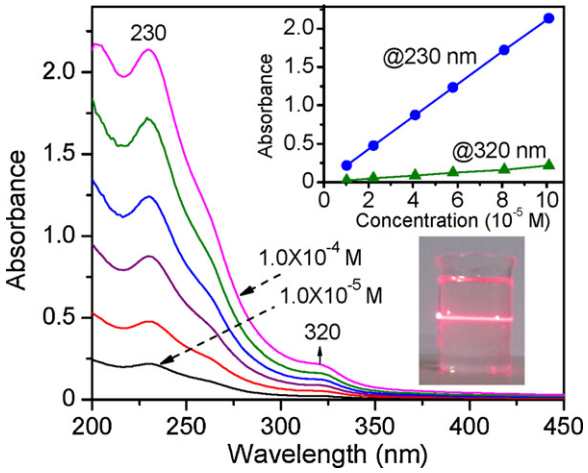

Fig. 5. UV–vis absorption spectrum of the colloidal suspension containing the exfoliated $La_{0.90}Dy_{0.05}Nb_2O_7$ nanosheets, where the relationship between the absorbance and the concentration is plotted in the top insert and a photograph of a colloidal suspension with the Tyndall scattering effect is shown in the bottom insert.

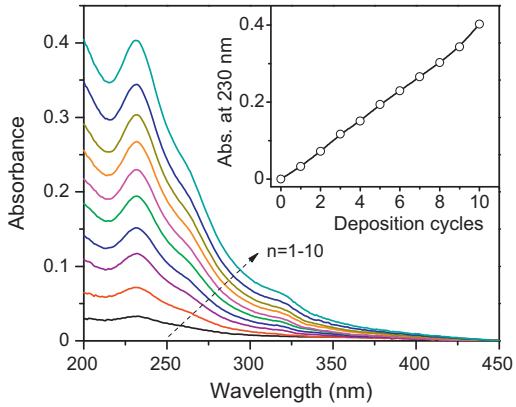

Fig. 6. UV–vis absorption spectra of the multilayer film $(PEI/La_{0.90}Dy_{0.05}Nb_2O_7)_{10}$ monitoring sequential deposition of number. The insert indicates the relationship between the absorbance at 230 nm and the deposition cycle.

3.3. Film fabrication

Employing a LBL assembly method, the multilayer was achieved by alternately immersed the substrate in a protonic PEI aqueous solution and a negatively charged nanosheet colloidal suspension. After repeating the dipping cycles several times, a transparent multilayer film composed of n layers of $(PEI/La_{0.90}Dy_{0.05}Nb_2O_7$ nanosheet$)_n$ was obtained. UV–vis absorption of the film was monitored immediately after each deposition cycle (Fig. 6). The nearly linear increase in peak absorbance at 230 nm with the deposition cycle n, as displayed in the top insert of Fig. 6, provides evidence for the successful multilayer buildup with approximately equivalent absorbance in each deposition cycle, confirming the stepwise growth of multilayer film.

The powder XRD pattern of the as-deposited $(PEI/La_{0.90}Dy_{0.05}Nb_2O_7)_{10}$ multilayer film is shown in Fig. 7a. The (0 1 0) reflection at $2\theta = 4.15^\circ$ with the intersheet distance of 2.13 nm can be ascribed to the nanostructure arising from the repeating PEI/nanosheet unit, close to that of $PEI/La_{0.90}Dy_{0.05}Nb_2O_7$ flocculation. Exposing the $(PEI/La_{0.90}Dy_{0.05}Nb_2O_7)_{10}$ multilayer film to UV light allowed the photocatalytic removal of the PEI moiety, due to the photocatalytical nature of the semiconductor nanosheets [1,34]. The intersheet distance was decreased with the UV light irradiation time (the insert of Fig. 7). After UV light exposure for 12 h, the peak was shifted to a higher angle 7.65° with

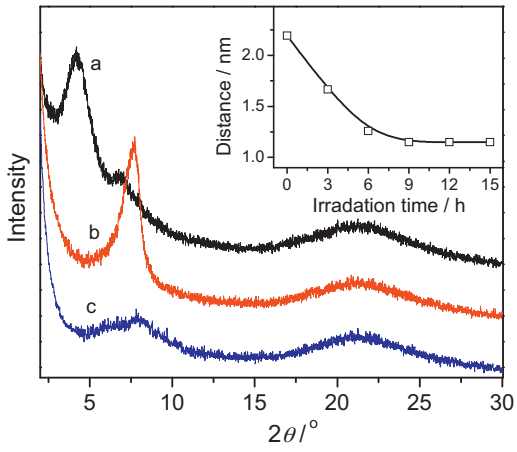

Fig. 7. XRD patterns for the multilayer films of $(PEI/La_{0.90}Dy_{0.05}Nb_2O_7)_{10}$: as-deposited (a), after UV light exposure for 12 h (b) and after heat-treated at 450 °C for 2 h (c). The intersheet distance is plotted against the UV light exposure time in the inset.

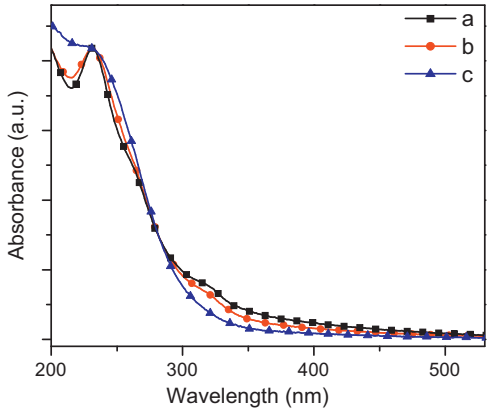

Fig. 8. Normalized absorption spectra of $(PEI/La_{0.90}Dy_{0.05}Nb_2O_7)_{10}$: as-deposited (a), after UV light exposure for 12 h (b) and after heat-treated at 450 °C for 2 h (c).

a duplicated distance of 1.15 nm between the nanosheets (Fig. 7b). This intersheet shrinkage can be explained as the degradation of the intercalated PEI polymer layer due to the photocatalytic activity of the lanthanoniobate nanosheets, similar to the $PDDA/Ti_{0.92}O_2$ and $PDDA/Nb_3O_8$ multilayer films [3,32]. On the other hand, after the $(PEI/La_{0.90}Dy_{0.05}Nb_2O_7)_{10}$ multilayer film was heated at 450 °C for 2 h to move the organic components, similar XRD profile was obtained, which exhibits a peak at $2\theta = 7.88°$ with d-spacing of 1.12 nm (Fig. 7c). The periodicity of 1.15 or 1.12 nm is similar to the thickness of lanthanoniobate nanosheet (1.13 nm) detected in the AFM analysis above and somewhat greater than the theoretic value (1.07 nm) [28]. The residue after the post-treatments was curtained as ammonium and/or oxonium ions in the intersheet galleries, along with some water molecules [3,19,31]. The broad peaks may be related with the misalignment of the nanosheet crystallites [20]. Such polymer-free multilayer films of $La_{0.90}Dy_{0.05}Nb_2O_7$ nanosheets allow us to perform the following PL experiments to avoid the possible interference with the intercalated polymer.

The comparison between the UV–vis absorption spectrum of $(PEI/La_{0.90}Dy_{0.05}Nb_2O_7)_{10}$ film and its corresponding post-treated samples is shown in Fig. 8. Since PEI shows negligible absorption in the measured wavelength range of 200–800 nm, the absorption profile of the nanosheet film is similar to that in the form of colloidal suspension. After UV light exposure for 12 h, no apparent change in UV–vis spectra was observed. In contrast, after heat treatment at 450 °C for 2 h, the peak at around 230 nm with respect to that for the as-prepared film was broadened, the broad peak at 320 nm disappeared and the absorption edge blue-shifted. As mentioned above, the heat treatment made more the residual species evaporate from the intersheet galleries, and introduced more lattice strain than that from the UV light exposure. The lattice strain would make the absorption edge blue-shifted.

3.4. Photoluminescence properties

The PL spectra of the bulk layered compound $KLa_{0.90}Dy_{0.05}Nb_2O_7$ and the protonated $HLa_{0.90}Dy_{0.05}Nb_2O_7$ are shown in Fig. 9. For these two phases, broad direct excitation from the lowest ground state $^6H_{15/2}$ to various $4f^5$ states of Dy^{3+} was observed, whereas no host excitation-mediated luminescence was observed at room temperature. The general observed peaks distribution due to the intra-4f transitions of Dy^{3+} is similar to those of Dy^{3+}-photoactivated phosphors [27,35]. Rosa et al. proposed that the high symmetry of the substitutional Dy^{3+} photoactivators in matrix lattice can lead to broad excitation peaks [27]. Therefore, the broad appearance of excitation peaks for the two present phases may suggest that the Dy^{3+} ions in $KLa_{0.90}Dy_{0.05}Nb_2O_7$ or $HLa_{0.90}Dy_{0.05}Nb_2O_7$ are mainly substituted at the La^{3+} sites with high symmetry, that is, at the 12-fold coordination sites of the La^{3+} cation within the $KLaNb_2O_7$ or $HLaNb_2O_7$ crystal lattice. As mentioned above, the UV–vis absorption peaks below 330 nm of the bulk compounds $KLa_{0.90}Dy_{0.05}Nb_2O_7$ and $HLa_{0.90}Dy_{0.05}Nb_2O_7$ were observed, due to the bandgap transitions (Fig. 3). The absence of this host excitation-mediated luminescence in the two present phases suggests the existence of significant nonradiative relaxation, as observed in Sm^{3+}-doped $KLaNb_2O_7$ bulk layered perovskite [12] and other Ln-doped oxides [36,37]. Excited at 388 nm, the emission spectra of the two present phases exhibit two main peaks, one in the blue region centered at 480 nm ($^4F_{9/2} \rightarrow {}^6H_{15/2}$) and the other one in the yellow region at 576 nm ($^4F_{9/2} \rightarrow {}^6H_{13/2}$), both characteristic of the Dy^{3+} photoactivator [38]. It is known that the $^4F_{9/2} \rightarrow {}^6H_{15/2}$ transition is a magnetic dipole transition, which is independent of the site symmetry at which Dy^{3+} ion is situated, while the $^4F_{9/2} \rightarrow {}^6H_{13/2}$ transition is an electric dipole transition, which is especially sensitive to its surrounding and is allowed only at low symmetries with no inversion center [25–27]. When the Dy^{3+} ion is located at a low-symmetric site, the hypersensitive transition (yellow, $^4F_{9/2} \rightarrow {}^6H_{13/2}$) is often prominent in its emission spectra [39]. As displayed in Fig. 9, the intensities of two emissions are nearly equivalent with each other, further indicating that the amount of Dy^{3+} into the interstitial or defect sites of $KLaNb_2O_7$ crystal structure is very small and that into the La^{3+} substitutional positions is prominent. The protonated bulk layered compound $HLa_{0.90}Dy_{0.05}Nb_2O_7$ exhibits similar emissions to the pristine $KLa_{0.90}Dy_{0.05}Nb_2O_7$.

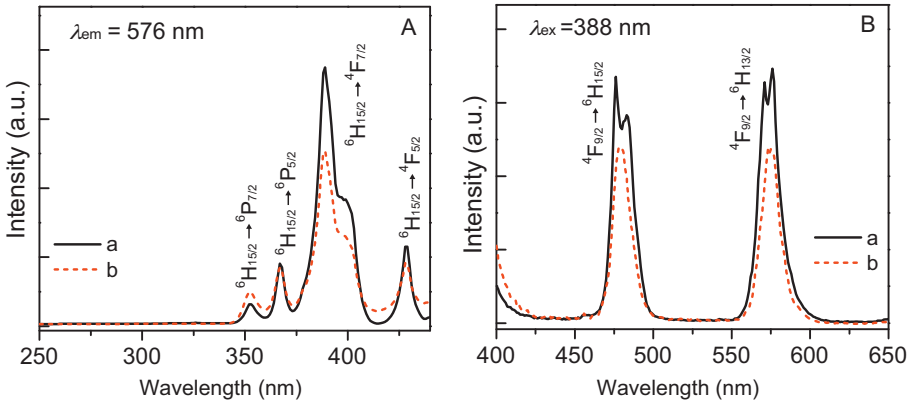

Fig. 9. Photoluminescence excitation (A) and emission (B) spectra of bulk precursors $KLa_{0.90}Dy_{0.05}Nb_2O_7$ (a) and $HLa_{0.90}Dy_{0.05}Nb_2O_7$ (b). The excitation spectra were monitored at 576 nm, and the emission spectra were obtained under excitation at 388 nm.

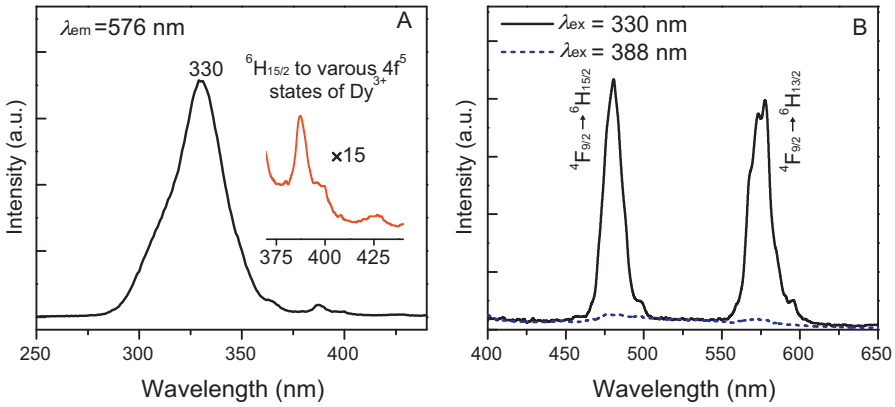

Fig. 10. Photoluminescence excitation (A) and emission (B) spectra of exfoliated $La_{0.90}Dy_{0.05}Nb_2O_7$ nanosheet. The excitation spectra were monitored at 576 nm, and the emission spectra were obtained under excitation at 330 and 388 nm, respectively. The inset in A indicates the enlarged excitation spectrum between 370 and 440 nm.

The PL spectra of the exfoliated $La_{0.90}Dy_{0.05}Nb_2O_7$ nanosheet in colloidal suspension (2×10^{-5} M) are shown in Fig. 10. The exfoliated nanosheet suspension exhibits the emission characteristic of Dy^{3+} photoactivator, the blue $^4F_{9/2} \rightarrow {}^6H_{15/2}$ transition centered at 480 nm and the yellow $^4F_{9/2} \rightarrow {}^6H_{13/2}$ transition centered at 573 nm. The slight shift of 3 nm for the $^4F_{9/2} \rightarrow {}^6H_{13/2}$ transition with respect to those of the bulk precursors is likely to be due to the different relative intensities of its Stark components rather than the nephelauxetic effect because of the covalent interaction strength difference between the activators and the hosts, similar to the case for $La_{0.90}Eu_{0.05}Nb_2O_7$ nanosheet [12]. However, the excitation spectrum of the exfoliated $La_{0.90}Dy_{0.05}Nb_2O_7$ nanosheet suspension is very different from those of the bulk compounds $KLa_{0.90}Dy_{0.05}Nb_2O_7$ and $HLa_{0.90}Dy_{0.05}Nb_2O_7$. A broad excitation band centered at 330 nm was clearly observed for the $La_{0.90}Dy_{0.05}Nb_2O_7$ nanosheet (Fig. 10A). This broad band considerably differs from the excitation spectrum of the bulk compounds, but closely resembles the bandgap absorption with a maximum at 320 nm (Fig. 5). Therefore, this broad excitation band cannot be attributed to the direct Dy^{3+} excitation transition [40,41], but it is likely based on the energy transfer from the bandgap excitation to the Dy^{3+} photoactivators within the nanosheet host. The O–Ln CT transition is likely to contribute to this excitation band, as suggested for other Ln-activated oxide phosphors [5,12–16,42,43]. Furthermore, the emission by direct Dy^{3+} excitation was significantly and preferentially quenched after exfoliation. The emission through host excitation is far more prominent than that through direct Dy^{3+} excitation for the $La_{0.90}Dy_{0.05}Nb_2O_7$ nanosheet.

It is well-known that photoluminescence intensity is related to the degree of the nonradiative relaxation process, which is largely affected by energy trapping [13,37]. A model for the energy transfer in the $La_{0.90}Dy_{0.05}Nb_2O_7$ nanosheet is proposed in Fig. 11. The fact that emission intensity from the direct excitation (process 2) of Dy^{3+} in the nanosheet is negligibly small suggests that the nonradiative relaxation through the excited 4f states of Dy^{3+} (processes 12 and 13) via trapping states has higher transition probability than that through host excitation (processes 11 and 13), and the host excitation-mediated processes 3 and 4 have relatively high transition probability. In the form of nanosheet suspension, the host excitation energy has to be transferred within the perovskite sheet and the intersheet energy migration should be minimized. Therefore, the exfoliated nanosheet has more efficient host to photoactivator energy transfer than its bulk precursors $KLa_{0.90}Dy_{0.05}Nb_2O_7$ and $HLa_{0.90}Dy_{0.05}Nb_2O_7$, which have considerable intersheet interactions and make nonradiative relaxation (processes 7–9) significant. The previous reported Ln-doped layered phosphors are consistent with this expectation [5,10–13,36,37]. It is noted that the nanosheet has far larger surface than those of the bulk layered compounds, which makes the nanosheet can absorb more energy and the energy must be easier transferred from the nanosheet host to the Dy^{3+} photoactivators than that in the bulk layered compounds. The nonradiative relaxation in the direct Dy^{3+} excitation-mediated processes is likely related to the energy trapping states, from which energy dissipates to the factors such as vibrations of surfactants. It was observed that such nonradiative relaxation channels are provided by the vibrations of the adsorbed species such as OH^-, H_2O or H_3O^+ in the Ln-photoactivated materials [5,12,36,37]. The large surface of the nanosheet makes such contribution from the adsorbed species significant, and subsequently results in the decreased emission intensity of the nanosheet. As shown in Fig. 10A, the host excitation-mediated emission has a greater intensity than the direct Dy^{3+} excitation-mediated emission. It indicates that the trapping state is positioned near the excited 4f states of Dy^{3+}, which elevates the probability of process 12 rather than 11.

The excitation spectra of the as-prepared $(PEI/La_{0.90}Dy_{0.05}Nb_2O_7)_{10}$ multiple film and its post-treated samples are displayed in Fig. 12A. Different from the bulk compounds $KLa_{0.90}Dy_{0.05}Nb_2O_7$ and $HLa_{0.90}Dy_{0.05}Nb_2O_7$ but similar to the exfoliated $La_{0.90}Dy_{0.05}Nb_2O_7$ nanosheet, each present material has a broad and intensive band between 240 and 350 nm from the host excitation-mediated luminescence and an almost indistinguishable form above 350 nm from the direct Dy^{3+} excitation. The intersheet interactions in these cases are expected to be weakened with respect to the bulk compounds $KLa_{0.90}Dy_{0.05}Nb_2O_7$ and

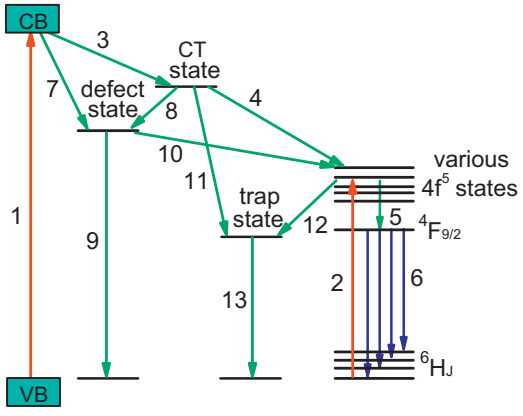

Fig. 11. A model for the energy transfer leading to photoluminescence in the $La_{0.90}Dy_{0.05}Nb_2O_7$ nanosheet system.

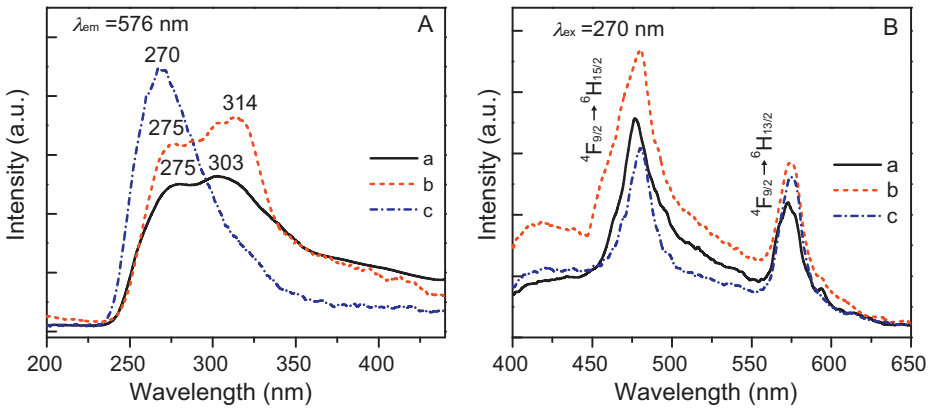

Fig. 12. Photoluminescence excitation (A) and emission (B) spectra of $(PEI/La_{0.90}Dy_{0.05}Nb_2O_7)_{10}$ films: as-deposited (a), after UV light exposure for 12 h (b) and after heat-treated at 450 °C for 2 h (c). The excitation spectra were monitored at 576 nm, and the emission spectra were obtained under excitation at 270 nm.

$HLa_{0.90}Dy_{0.05}Nb_2O_7$, and the intersheet energy migration associated with the nonradiative relaxation (processes 7–9) thus be reduced. On the other hand, the adsorption properties of the films are expected to be similar to that of the nanosheet, which makes the nonradiative relaxation through the direct Dy^{3+} excitation (processes 12 and 13) significant. These factors make the host excitation prominent. The as-deposited $(PEI/La_{0.90}Dy_{0.05}Nb_2O_7$ nanosheet$)_{10}$ multilayer film shows two main peaks at 275 and 303 nm in its excitation spectrum. Two peaks at 275 and 314 nm were observed after UV light exposure and only one main peak at 270 nm was observed after heat-treatment at 450 °C. These excitation peaks coincide with their bandgap absorptions (Fig. 8). As mentioned above, the bands centered at 230 and 320 nm in their UV–vis absorption spectra are originated from the transitions through the valence band (VB), composed of the 2p orbits in O^{2-}, to the conduction band (CB) components composed of the 3d orbits in Nb^{5+} and the 4d and 4f orbits in Ln^{3+}, respectively. Therefore, the excitation peaks at around 270 nm are attributed to the energy transfer from the Nb–O network to Dy^{3+} in the nanosheet host and the broad excitation bands between 303 and 330 nm are likely based on the energy transfer from the bandgap excitation to the Dy^{3+} photoactivators through the O–Dy CT transition, similar to other Ln-activated nanosheet phosphors [5]. The transition probability from the Nb–O network to Dy^{3+} may be related to the different defect states in these materials. Stronger lattice strain was introduced after heat treatment, which makes the energy transfer more effective and this excitation sharper and more intensive [36,44,45]. Electrons promoted to CB decay nonradioactively to the recombination band associated to the traps produced by the presence of defects [27,44]. From this metastable band electrons decay to VB and produce the broad emission.

The Dy^{3+} characteristic emission in the as-prepared $(PEI/La_{0.90}Dy_{0.05}Nb_2O_7)_{10}$ multiple film and its post-treated samples give two emission peaks and the blue emission ($^4F_{9/2} \rightarrow {}^6H_{15/2}$) is prominent. The emission peaks exhibit slight shifts with respect to the bulk precursors and the nanosheet suspension. Their blue $^4F_{9/2} \rightarrow {}^6H_{15/2}$ transition are centered between 477 and 480 nm and their yellow $^4F_{9/2} \rightarrow {}^6H_{13/2}$ transition between 572 and 576 nm. Like the case for $La_{0.90}Eu_{0.05}Nb_2O_7$ nanosheet [12], these slight shifts are proposed to be due to the different relative intensities of its Stark components. As mentioned above, if the Dy^{3+} site has high symmetry, the electric dipole emission ($^4F_{9/2} \rightarrow {}^6H_{13/2}$) is weak and the magnetic dipole transition ($^4F_{9/2} \rightarrow {}^6H_{15/2}$) becomes relatively stronger. The ratio between the two transitions I_{yellow}/I_{blue} is a measure of the site asymmetry in which the Dy^{3+} is situated. The ratios for the as-prepared $(PEI/La_{0.90}Dy_{0.05}Nb_2O_7)_{10}$ multiple film and its post-treated samples after UV light exposure for 12 h and after heat-treated at 450 °C for 2 h are 0.63, 0.61 and 0.85, respectively. These values are lower than those of $KLa_{0.90}Dy_{0.05}Nb_2O_7$ (1.03), $HLa_{0.90}Dy_{0.05}Nb_2O_7$ (0.99) and the $La_{0.90}Dy_{0.05}Nb_2O_7$ nanosheet (0.93). In general, the surrounding of Dy^{3+} in the $La_{0.90}Dy_{0.05}Nb_2O_7$ lattice be possibly influenced by the factors such as the introduced defects, the local adsorption of chemical species and the physical lattice distortion, similar in Dy^{3+}-activated nanoparticles [27,36,44,45]. The observations indicate that the symmetry of the Dy^{3+} sites might increase in the film forms and that the factors can put into effects much more easily in a nanosheet and its films than in the parent bulk materials, which makes the I_{yellow}/I_{blue} ratio decreased. The larger distortion after heat treatment gave a greater increase in the blue emission.

4. Conclusions

In the present paper, the Dy^{3+}-activated perovskite nanosheet, $La_{0.90}Dy_{0.05}Nb_2O_7$, was achieved by chemically exfoliating the layered perovskite $KLa_{0.90}Dy_{0.05}Nb_2O_7$ and the exfoliated nanosheets were assembled into multilayer films using the LBL electrostatic deposition technology. The $La_{0.90}Dy_{0.05}Nb_2O_7$ nanosheet and its multilayer films exhibit intense emission by the host excitation and negligibly low emission by the direct Dy^{3+} excitation, while the photoluminescence emissions of the bulk precursors are largely dominated by the direct Dy^{3+} excitation rather than the host excitation. The relative enhancement of the host excitation-mediated photoluminescence of $La_{0.90}Dy_{0.05}Nb_2O_7$ nanosheet is based on the energy transfer from the efficient O–Dy CT transition to Dy^{3+}, and the enhanced emission of the multilayer films is attributed to the efficient energy transfer from both of the O–Dy CT transition and the O–Nb network to Dy^{3+}. Dy^{3+} in the $La_{0.90}Dy_{0.05}Nb_2O_7$ nanosheet and the nanosheet-based films gives two emission peaks and the blue emission is prominent in the films. It is much important to modulate the excitation and emission wavelengths for many of the practical phosphor applications. Based on this relative enhancement of the host excitation-mediated photoluminescence by exfoliating bulk Ln-photoactivated layered phosphors into nanosheets and assembling nanosheets into multilayer films, it is expected to develop a new approach for designing practical phosphor materials.

Acknowledgments

This work was supported by National Natural Science Foundation of China (50872037, 21003055, 21103054), Natural Science

Foundation of Fujian Province (2010J01040) and Program for New Century Excellent Talents in Fujian Province University (06FJR01).

References

[1] R. Ma, T. Sasaki, Adv. Mater. 22 (2010) 5082.
[2] T. Sasaki, M. Watanabe, H. Hashizume, H. Yamada, H. Nakazawa, J. Am. Chem. Soc. 18 (1996) 8329.
[3] N. Sakai, Y. Ebina, K. Takeda, T. Sasaki, J. Am. Chem. Soc. 126 (2004) 5851.
[4] R.E. Schaak, T.E. Mallouk, Chem. Mater. 12 (2000) 2513.
[5] S. Ida, C. Ogata, M. Eguchi, W.J. Youngblood, T.E. Mallouk, Y. Matsumoto, J. Am. Chem. Soc. 130 (2008) 7052.
[6] K. Maeda, T.E. Mallouk, J. Mater. Chem. 19 (2009) 4813.
[7] B.H. Xu, B.Z. Lin, Q.Q. Wang, O. Zhang, L.M. Fu, H. Liu, Micropor. Mesopor. Mater. 147 (2012) 79.
[8] H. Tetsuka, T. Ebina, F. Mizukami, Adv. Mater. 20 (2008) 3039.
[9] X.L. Li, B.Z. Lin, B.H. Xu, Z.J. Chen, Q.Q. Wang, J.D. Kuang, H. Zhu, J. Mater. Chem. 20 (2010) 3924.
[10] S. Ida, C. Ogata, U. Unal, K. Izawa, T. Inoue, O. Altuntasoglu, Y. Matsumoto, J. Am. Chem. Soc. 129 (2007) 8956.
[11] T.C. Ozawa, K. Fukuda, K. Akatsuka, Y. Ebina, T. Sasaki, K. Kurashima, K. Kosuda, J. Phys. Chem. C 112 (2008) 1312.
[12] T.C. Ozawa, K. Fukuda, K. Akatsuka, Y. Ebina, T. Sasaki, Chem. Mater. 19 (2007) 6575.
[13] T.C. Ozawa, K. Fukuda, K. Akatsuka, Y. Ebina, K. Kurashima, T. Sasaki, J. Phys. Chem. C 113 (2009) 8735.
[14] T.C. Ozawa, K. Fukuda, K. Akatsuka, Y. Ebina, T. Sasaki, K. Kurashima, K. Kosuda, J. Phys. Chem. C 112 (2008) 17115.
[15] T.C. Ozawa, K. Fukuda, Y. Ebina, K. Kosuda, A. Sato, Y. Michiue, K. Kurashima, T. Sasaki, Sci. Technol. Adv. Mater. 12 (2011) 044601.
[16] A. Kudo, Chem. Mater. 9 (1997) 664.
[17] S. Neeraj, N. Kijima, A.K. Cheetham, Chem. Phys. Lett. 387 (2004) 2.
[18] S. Ida, K. Araki, U. Unal, K. Izawa, O. Altuntasoglu, C. Ogata, Y. Matsumoto, Chem. Commun. (2006) 3619.
[19] T. Sasaki, Y. Ebina, T. Tanaka, M. Harada, M. Watanabe, G. Decher, Chem. Mater. 13 (2001) 4661.
[20] H. Tetsuka, H. Takashima, K. Ikegami, H. Nanjo, T. Ebina, F. Mizukami, Chem. Mater. 21 (2009) 21.
[21] L. Wang, T. Sasaki, Y. Ebina, K. Kurashima, M. Watanabe, Chem. Mater. 14 (2002) 4827.
[22] T. Sasaki, Y. Ebina, K. Fukuda, T. Tanaka, M. Harada, M. Watanabe, Chem. Mater. 14 (2002) 3524.
[23] J. Huang, R. Ma, Y. Ebina, K. Fukuda, K. Takada, T. Sasaki, Chem. Mater. 22 (2010) 2582.
[24] T. Shibata, G. Takanashi, T. Nakamura, K. Fukuda, Y. Ebina, T. Sasaki, Energy Environ. Sci. 4 (2011) 535.
[25] A. Zhang, M. Lü, G. Zhou, S. Wang, Y. Zhou, J. Phys. Chem. Solids 67 (2006) 2430.
[26] N. Maruyama, T. Honma, T. Komatsu, J. Solid State Chem. 182 (2009) 246.
[27] L.A. Diaz-Torres, E. De la Rosa, P. Salas, V.H. Romero, C. Angeles-Chavez, J. Solid State Chem. 181 (2008) 75.
[28] M. Sato, J. Abo, T. Jin, M. Ohta, Solid State Ionics 51 (1992) 85.
[29] M. Sato, J. Abo, T. Jin, M. Ohta, J. Alloys Compd. 192 (1993) 81.
[30] X.T. Pian, B.Z. Lin, Y.L. Chen, J.D. Kuang, K.Z. Zhang, L.M. Fu, J. Phys. Chem. C 115 (2011) 6531.
[31] Q.Q. Wang, B.Z. Lin, B.H. Xu, X.L. Li, Z.J. Chen, X.T. Pian, Micropor. Mesopor. Mater. 130 (2010) 344.
[32] Z. Liu, R. Ma, M. Osada, N. Iyi, Y. Ebina, K. Takada, T. Sasaki, J. Am. Chem. Soc. 128 (2006) 4872.
[33] Y. Matsumoto, M. Koinuma, Y. Iwanaga, T. Sato, S. Ida, J. Am. Chem. Soc. 131 (2009) 6644.
[34] K.K. Manga, Y. Zhou, Y. Yan, K.P. Loh, Adv. Funct. Mater. 19 (2009) 3638.
[35] X. Fu, S. Niu, H. Zhang, Q. Xin, Mater. Sci. Eng. B 129 (2006) 14.
[36] S. Jeon, P.V. Braun, Chem. Mater. 15 (2003) 1256.
[37] W. Di, X. Wang, P. Zhu, B. Chen, J. Solid State Chem. 180 (2007) 467.
[38] G. Dominiak-Dzik, W. Ryba-Romanowski, M.N. Palatnikov, N.V. Sidorov, V.T. Kalinnikov, J. Mol. Struct. 704 (2004) 139.
[39] M. Yu, J. Lin, Z. Zhang, J. Fu, S. Wang, H.J. Zhang, Y.C. Han, Chem. Mater. 14 (2002) 2224.
[40] H. Lin, D. Yang, G. Liu, T. Ma, B. Zhai, Q. An, J. Yu, X. Wang, X. Liu, Y.B. Pun, J. Lumin. 113 (2005) 121.
[41] L. An, J. Zhang, M. Liu, S. Chen, S. Wang, Opt. Mater. 30 (2008) 957.
[42] Q.Y. Zhang, K. Pita, W. Ye, W.X. Que, Chem. Phys. Lett. 351 (2006) 163.
[43] Y. Zhou, J. Lin, S. Wang, J. Solid State Chem. 171 (2003) 391.
[44] E. De la Rosa-Cruz, L.A. Díaz-Torres, P. Salas, R.A. Rodríguez, G.A. Kumar, M.A. Meneses, J.F. Mosino, J.M. Hernández, O. Barbosa-García, J. Appl. Phys. 94 (2003) 3509.
[45] P. Salas, C. Angeles, J.A. Montoya, E. De la Rosa, L.A. Díaz-Torres, A. Martínez, M.A. Romero-Romo, J. Morales, Opt. Mater. 27 (2005) 1295.